Progress in Natural Science: Materials International 2013;23(3):317–325

Chinese Materials Research Society

Progress in Natural Science: Materials International

www.elsevier.com/locate/pnsmi
www.sciencedirect.com

ORIGINAL RESEARCH

Synthesis of Au–Ag alloy nanoparticles supported on silica gel via galvanic replacement reaction

Xiaoyan Liu[a,b], Aiqin Wang[a], Lin Li[a], Tao Zhang[a,*], Chung-Yuan Mou[b,], Jyh-Fu Lee[c]**

[a]*Dalian Institute of Chemical Physics, Chinese Academy of Sciences, 457 Zhongshan Road, Dalian 116023, China*
[b]*Department of Chemistry, National Taiwan University, Taipei 10617, Taiwan*
[c]*National Synchrotron Radiation Research Center, Hsinchu 30076, Taiwan*

Received 2 September 2012; accepted 26 March 2013
Available online 17 May 2013

KEYWORDS

Gold;
Silver;
Alloy;
XAS;
Galvanic replacement reaction

Abstract Synthesis of supported Au–Ag bimetallic has attracted much attention since we found for the first time that Au and Ag had synergistic effect on CO oxidation and preferential CO oxidation in rich hydrogen. In this work, the formation of Au–Ag alloy nanoparticles supported on silica gel by galvanic replacement reaction has been investigated. We applied various characterizations including X-ray diffraction (XRD), transmission electronic microscopy (TEM), ultraviolet–visible spectroscopy (UV–vis), X-ray absorption spectroscopy (XAS) to characterize the formation process of Au–Ag alloy. Although the average particle sizes of the Au–Ag alloy nanoparticles obtained by the galvanic replacement reaction are relatively large comparing with that of loading Au first, the catalytic activity of the catalyst in preferential CO oxidation is almost the same. This result manifested that the particle size effect of Au–Ag nanoparticles was not as tremendous as that of monometallic gold. The formation of Au–Ag alloy made it less sensitive to the particle size.

1. Introduction

Au and Ag have the same face centered cubic (fcc) structure and lattice spacings, and they easily form alloy phase [1]. In many functional properties, the performances of Au–Ag alloy nanoparticles are superior to the corresponding monometallic ones, such as in surface enhanced Raman spectroscopy (SERS) [2–4], sensors [5,6], and catalysis [7,8]. Therefore, many synthesis approaches of bimetallic Au–Ag nanoparticles have been developed, such as digestive ripening [9], laser synthesis method [10], seed growth

*Corresponding author. Tel.: +86 411 84379015; fax: +86 411 84691570.
**Corresponding author. Tel.: +886 2 33665251; fax: +886 2 23660954.
E-mail addresses: taozhang@dicp.ac.cn (T. Zhang), cymou@ntu.edu.tw (C.-Y. Mou).

Peer review under responsibility of Chinese Materials Research Society.

Production and hosting by Elsevier

1002-0071 © 2013 Chinese Materials Research Society. Production and hosting by Elsevier B.V. All rights reserved.
http://dx.doi.org/10.1016/j.pnsc.2013.04.008

method [11], ligand binding method [12–14], and galvanic reaction [15]. Since the seminal discovery of catalytic activity by gold nanoparticles, supported Au–Ag alloy nanoparticles have been receiving increasing attentions for possible enhancement in catalytic activity [16]. In 2005, we reported that Au and Ag showed obvious synergetic effect in CO oxidation reaction over an alloy nanocatalyst Au–Ag@MCM-41 catalyst [17]. Since then, the Au–Ag alloy system has been applied to various reactions including oxidation of alcohols [7,18], acetylene hydrogenation [19] and photocatalytic reaction [8,20].

Since the standard solution sources of Au and Ag ($HAuCl_4$ and $AgNO_3$) are immiscible due to the formation of AgCl, synthesis of highly dispersed Au–Ag alloy nanoparticles is challenging especially on inert support such as silica. Previously, we developed a one-pot method to prepare Au–Ag@MCM-41 by using the surfactant hexadecyltrimethylammonium bromide (CTAB) as both template for MCM-41 and protecting agent for making Au–Ag alloy nanoparticles [17,21–23]. However, the formation of AgBr led to the agglomeration of the particles and the average particle size is relatively large (20–30 nm). They were much bigger than the optimum size of supported gold catalysts (3–5 nm). Then, we further developed a two-step method to synthesize highly dispersed Au–Ag alloy nanoparticles supported on inert support such as SiO_2 and Al_2O_3 [24,25] by depositing gold on the support first and silver in the second step. The Cl^- was washed off during the first step and addition of Ag increased the stability of gold, the resulting Au–Ag alloy nanoparticles remained at about 3 nm even after high temperature calcination and reduction. Sandoval et al. investigated the Au–Ag alloy nanoparticles supported on TiO_2 by a sequential precipitation-deposition method, where they deposited Ag first and Au at the second step, and found that Au–Ag alloy nanoparticles are also very stable under high temperature pretreatment [26]. However, the effect of the deposition sequence on the formation of Au–Ag bimetallic nanoparticles supported on SiO_2 and their catalytic performances have not been investigated yet. Since Sun et al. found the replacement reaction method could synthesize Au–Ag bimetallic systems [27], various Au–Ag nanostructures have been developed including hollow cubes [15], porous surfaces [28] and alloy nanoparticles [29]. In this work, the formation of Au–Ag alloy nanoparticles by galvanic replacement reaction is studied by employing a reversed loading sequence compared with our previous work [24,25]. Various characterizations including XRD, TEM, UV–vis and XAS are employed to characterize the formation mechanism of Au–Ag alloy. The preferential CO oxidation in rich hydrogen (PROX) is chosen as a probe reaction to study the catalytic performance of the Au–Ag/SiO_2 catalyst. Based on these results, the formation mechanisms and intrinsic origin of the catalytic activity are discussed.

2. Experimental

2.1. *Preparation of the Au–Ag/SiO_2 catalyst*

We developed a two-step method to synthesize Au–Ag alloy nanoparticles supported on silica gel, where we support gold nanoparticles first, followed by deposition of silver in the second step [24,25]. Here, we prepare Au–Ag/SiO_2 in an inverse sequence, as shown in Fig. 1. In brief, the silica gel (Qingdao Ocean Chemical Plant, $S_{BET}=467\ m^2/g$) was first functionalized by APTES (3-aminopropyltriethoxysilane, $H_2N(CH_2)_3Si(OC_2H_5)_3$, Acrös). In the first step, silver was supported onto the support. 1.0 g of APTES-functionalized silica gel (APTES-SiO_2) was dispersed into 16 mL of deionized water followed by the addition of 4 mL of $AgNO_3$ solution (0.84 wt%) under continuous stirring. After 30 min, the mixture was filtered and washed. The recovered precursor was re-dispersed in 20 mL of $NaBH_4$ solution (0.1 M) and stirred for another 20 min. The mixture was filtered and washed again. The initially formed Ag particles were denoted as (a). Gold was deposited onto Ag-loaded support in the second step which is similar to the first one except that the metal precursor was changed to $HAuCl_4$ solution (4 mL, 1.65 wt%). When the $HAuCl_4$ was loaded onto the support, the mixture was filtered and washed till there was no Cl^- detected by $AgNO_3$. The sample was denoted as (b). After reduction with $NaBH_4$, the sample was denoted as (c). Samples (a–c) were all dried at room temperature before further characterization. After sample (c) was calcined at 500 °C in air, the sample was denoted as (d). When followed by further reduction at 550 °C under H_2, the sample was denoted as (e). Sample (a–e) defined above will be used in the whole article except that was described specially. The nominal atomic ratio of Au/Ag was 1, but the actual mole ratio obtained by inductively coupled plasma (ICP) was 1.3.

2.2. *Characterizations*

The actual loadings of the catalysts were determined by inductively coupled plasma spectrometer (ICP-AES) on an IRIS Intrepid II XSP instrument (Thermo Electron Corporation). The XRD patterns were collected on a PW3040/60 X' Pert PRO (PANalytical) diffractometer using a continuous mode from 20° to 80° at a scanning speed of 5°/min. The diffractometer was operated at 40 kV and 40 mA using Cu Kα radiation source ($\lambda=0.15432$ nm).

HRTEM images were obtained with a Tecnai G^2 F30 S-Twin transmission electron microscope operating at 300 kV. A few droplets of a suspension of the sample in ethanol were put on a microgrid carbon polymer supported on a copper grid and allowed to dry at room temperature for HRTEM observations. The particle size distribution was obtained by measuring more than 200 particles from randomly selected areas. UV–vis spectra were recorded at room temperature on a Cintra (GBC) apparatus with $BaSO_4$ as a reference.

In situ X-ray absorption spectroscopy (XAS) at Au L_{III}-edge and Ag K-edge were recorded at beamline 17C1 and 01C1 of National Synchrotron Radiation Research Center, Hsinchu, Taiwan. The electron storage ring is operated at 1.5 GeV and a beam current of 360 mA with a top-up injection mode. The beamline employs a double Si(111)-crystal monochromator for energy selection with a resolution $\Delta E/E$ better than 2×10^{-4}. The powdery catalysts were packed into the middle part of a quartz glass tube. Both ends of the tube are sealed with Kapton film. The reducing gas is pure H_2. All spectra were recorded at room temperature in a transmission mode. Au foil or Ag foil as standard was measured simultaneously by using a third ionization chamber so that energy calibration could be performed scan by scan. The X-ray absorption data were processed by Athena and Artemis software package [30].

2.3. *Catalytic test*

The catalytic activity for preferential CO oxidation in rich H_2 was measured using a continuous flow fixed-bed reactor system. A feed gas containing 1.0 vol% CO and 0.5 vol% O_2 and 50 vol% H_2 balanced

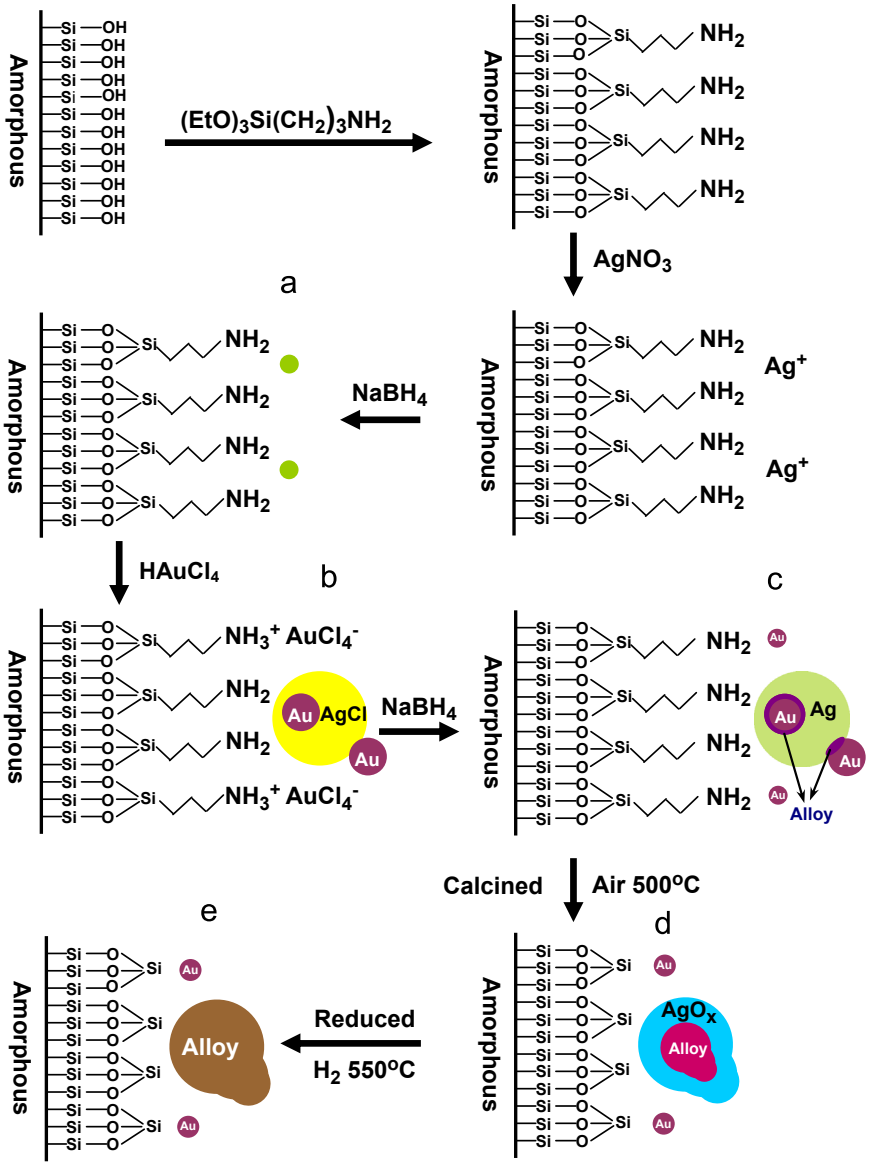

Fig. 1 Schematic illustration of the procedures for synthesis of SiO_2-supported Au–Ag alloy nanoparticles. (a) Initially formed Ag particles; (b) AgCl and Au obtained by replacement reaction between $HAuCl_4$ and Ag; (c) Au nanoparticles and Au–Ag alloy nanostructure in or on the interface of silver nanoparticles produced by reduction with $NaBH_4$; (d) slightly aggregated Au nanoparticles and Au–Ag nanostructure with more gold-rich alloy in the silver oxide species nanoparticles; and (e) Au nanoparticles and random alloy of Au–Ag nanoparticles on SiO_2 support.

with He passed through the catalyst sample of 60 mg (20–40 mesh) at a flow rate of 40 mL min^{-1} (corresponding to a space velocity of 40,000 mL h^{-1} g_{cat}^{-1}). Prior to the reaction, the catalyst was pretreated with H_2 at 550 °C for 1 h and then cooled to room temperature under He. The compositions of the inlet and outlet gas were online analyzed by a gas chromatograph (HP 6890, TDX-01 column).

3. Results

In Fig. 1, we not only show the experimental steps involved in making the Au–Ag nanoparticles supported on silica but also the detailed formation mechanism. In the followings, we will show detailed characterizations of the resulting nanocatalyst to support the mechanism. We will also evaluate the catalytic activity in PROX reaction.

3.1. *XRD patterns of the Au–Ag/SiO_2 catalyst*

We investigated the phase evolution at each step by XRD, as shown in Fig. 2. After Ag was loaded onto the surface of silica, there was no obvious diffraction peaks (Fig. 2a), which indicated that the Ag was highly dispersed or the actual loading of Ag was too low to be detected. After $HAuCl_4$ was introduced, an obvious signal of AgCl ($2\theta = 27.8°$, 32.4°, 46.3°, 54.8°, 57.5°) and XRD peaks for elemental Au ($2\theta = 38.2°$, 44.3°, 64.5°, 77.6°) appeared (Fig. 2b). Because the standard reduction potential of AgCl/Ag pair (0.22 V vs the standard hydrogen electrode, SHE) is lower than that of $AuCl_4^-$/Au (0.99 V vs SHE) [31], the reduction of Au (III) by Ag occurred when silver was first prepared on the silica surface (Reaction (3) in Section 4.1). The nominal atomic ratio of Au/Ag was 1.3, therefore, all the Ag could be consumed by galvanic replacement reaction with $AuCl_4^-$. The residual $AuCl_4^-$ (~67%)

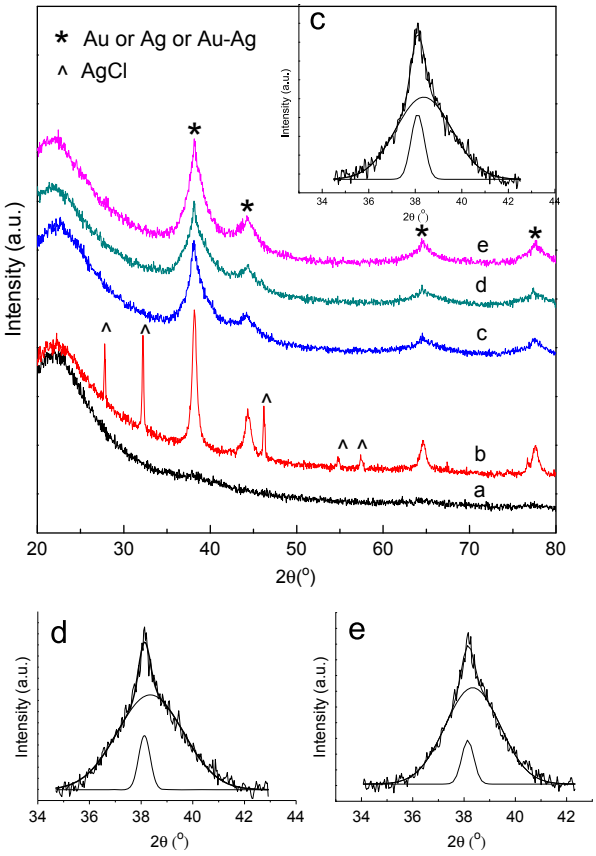

Fig. 2 XRD patterns of Au–Ag/SiO_2: (a–e) corresponding to those in Fig. 1.

then interacted with the –NH_2 on the surface of silica, as shown in Fig. 1b. The average particle size of Au obtained by galvanic replacement reaction by Ag was 11.7 nm, which was calculated from the half peak-width of the diffraction peak according to Scherrer equation. After being reduced by $NaBH_4$, the diffraction pattern of AgCl disappeared while the diffraction peaks of Au produced a broadened component in addition to the original sharp component. This indicated there appeared two sizes of gold nanoparticles at this stage. The diffraction patterns of Au (111) were fitted with two Gaussian curves (Fig. 2c) [32], and the calculated average particle sizes according to the Scherrer equation are 2.9 nm and 11.9 nm (Fig. 2c). In process c of Fig. 1, the AgCl and residual $AuCl_4^-$ were reduced to metallic Ag and Au, respectively. However, the space lattice of Au(111) and Ag(111) are very similar (0.408 nm and 0.409 nm, respectively) [21], their diffraction patterns at $2\theta = 38.2^\circ$ are overlapped. After calcinations at 500 °C and reduction at 550 °C, the XRD patterns did not change. Fig. 2d and e are very similar to Fig. 2c. The average particle sizes are 2.8 nm and 15.2 nm (Fig. 2d) and 3.3 nm and 14.4 nm (Fig. 2e), respectively.

3.2. *TEM images of the Au–Ag/SiO_2 catalyst*

We applied TEM to characterize the size distribution of the catalysts during the synthesis process. As shown in Fig. 3(a–e). In Fig. 3a, we found that most of the Ag nanoparticles were highly dispersed on the surface of silica, which is in good agreement with the XRD results in Fig. 2a. After galvanic replacement reaction occurred between Ag and $HAuCl_4$, nanoparticles with size ranging from about 2 to 50 nm were formed (Fig. 3b), which can be ascribed to the AgCl and Au. From Fig. 3c, we can see many small nanoparticles formed, which contributed to the wide diffraction peak in Fig. 2c. At the same time, the big ones still existed, which contributed to the sharp XRD peak in Fig. 2c. The particle size did not change much during the following steps as shown in Fig. 3d and e. The size distribution of sample (e) is shown in Fig. 3f. It had a much wider size distribution than that of Au–Ag alloy nanoparticles in our previous work [25]. The average particle size of the Au–Ag nanoparticles was 7.0 nm with a standard deviation of 4.2 nm, which indicated the size of the particles was composed of both small and big ones, which is consistent with the XRD result in Fig. 2e.

3.3. *UV–vis spectra of the Au–Ag/SiO_2 catalyst*

As we mentioned above, Au and Ag nanoparticles have the same face centered (fcc) structure and similar space lattices, we cannot ascertain the formation of Au–Ag alloy from XRD or TEM measurements. Here, we applied UV–vis to characterize the formation of Au–Ag alloy, as shown in Fig. 4. The absorption peak of monometallic Ag/SiO_2 positioned at 406 nm (Fig. 4a). This peak disappeared in step b, instead, a new absorption peak at 550 nm appeared (Fig. 4b), which was due to the surface plasma resonance band of Au nanoparticles. This indicates that the Ag was consumed to give Au nanoparticle by the galvanic replacement reaction, which is in good agreement with the XRD result in Fig. 2b. After reduction by $NaBH_4$, the absorption peak became wider and blue shifted to 525 nm and a new peak at 406 nm appeared simultaneously (Fig. 4c). This indicates the AgCl and the residual $AuCl_4^-$ were reduced to metallic state and formed Au–Ag alloy. The broadness of the peak indicates that the newly formed nanoparticles were much smaller (~3 nm) than those produced in step b. After calcined at 500 °C in air, there was only one peak positioned at 520 nm (Fig. 4d), which could be ascribed to the Au–Ag alloy phase with slightly Au-rich. Finally, we reduced the restored solid at 550 °C in pure H_2 and found the absorption peak was blue shifted to 468 nm (Fig. 4e) which implied the formation of Au–Ag alloy nanoparticles with larger ratio of Ag. We highlighted the Au–Ag alloy with different Au/Ag ratios in different colors, as shown in Fig. 1(c–e)

3.4. *XAS of the Au–Ag/SiO_2 catalyst*

The extended XAS is a powerful tool that can provide the structural information on the Au–Ag alloy. In order to obtain more specific details about the geometric and electronic environment of Au and Ag, we performed in situ XAS characterization of Au–Ag/SiO_2 catalyst. From Table 1 and Fig. 5(C–D)a, we can see, when Ag was deposited on the support first, the total coordination number (*CN*) of Ag in the first step was 5.4, which is much smaller than that of the Ag foil (*CN* = 12). This meant that the average particle size of Ag was very small [33]. Part of the Ag interacted with O, which was caused by exposure to air during the sample transfer and the experiment process. In step b, AgCl and Au were produced by galvanic replacement reaction between $HAuCl_4$ and Ag, as shown in Fig. 5(A–D)b. The fitted *CN* of Au was close to that of Au foil, which indicated that the particle size was relatively large [34]. This result is in good agreement with the XRD and TEM results in Figs. 2b and 3b. The distance between the Ag–Ag in AgCl was 3.06, which was longer than that of Ag foil. This

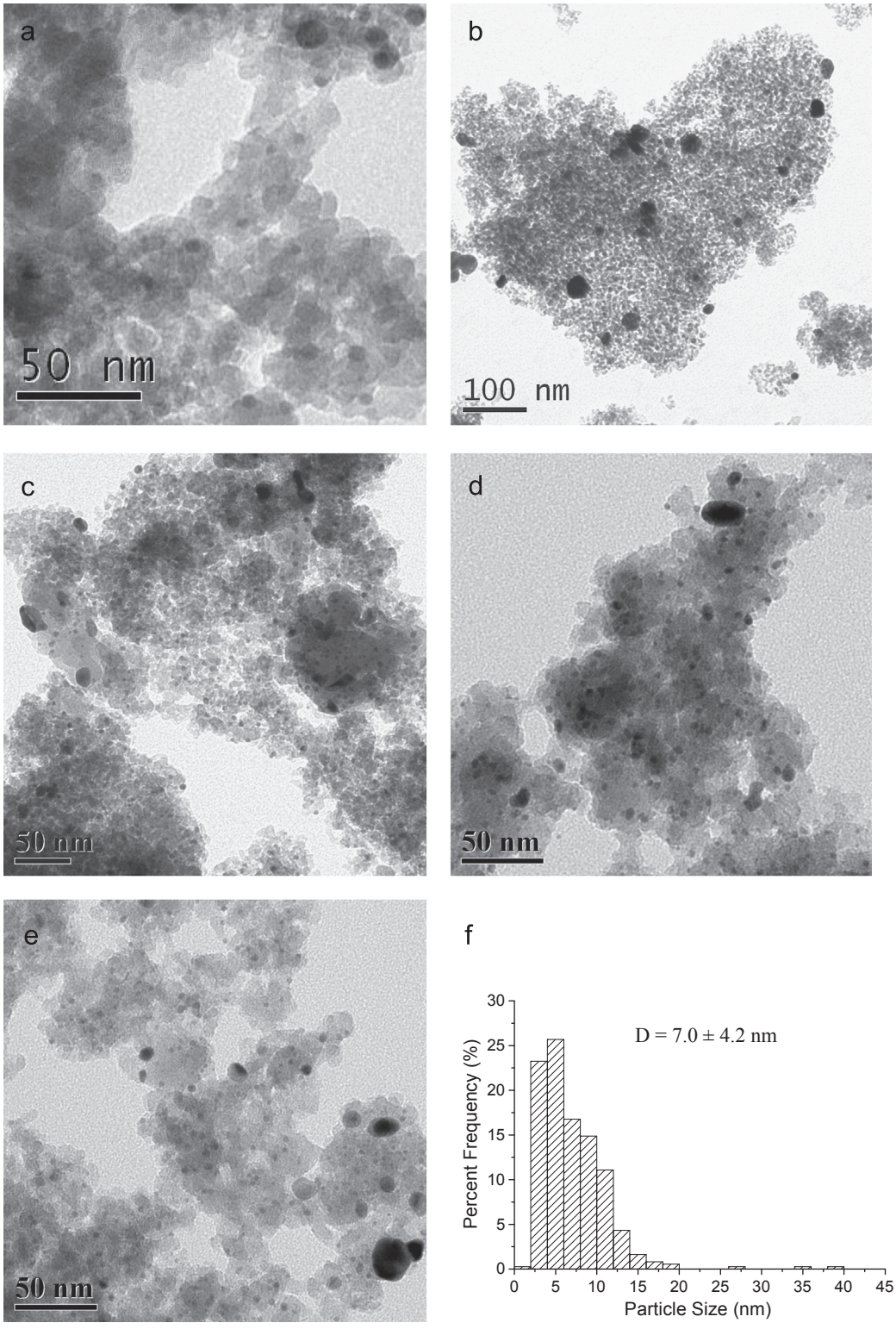

Fig. 3 TEM images of Au–Ag/SiO_2: (a–e) are corresponding to those in Fig. 1; and (f) the size distribution of sample (e).

result also manifested that the Ag was converted to AgCl via galvanic replacement reaction between $HAuCl_4$ and Ag, which is in good agreement with the XRD and UV–vis results. In step c, after reduction by $NaBH_4$ aqueous solution, AgCl and $AuCl_4^-$ were reduced to Ag and Au, respectively. According to Fig. 5(C–D)c and the data fitting results in Table 1, Au–Ag alloy formed at this step. The *CN* of Au–Ag and Ag–Au were 1.1 and 2.3 (Table 1), respectively. This is in good agreement with the UV–vis result (Fig. 4c). The small fraction of Ag–O interaction may be due to the oxidation of silver by air during the drying process. After calcination in air, as shown in Fig. 5(C–D)d Au–Ag alloy phase remained with some Ag interacting with O at the same time. Since

Ag_2O could be decomposed to Ag and O_2 after being calcined at temperatures higher than 150 °C, most of the Ag remained at metallic state according to the results of the EXAFS data in Table 1: the *CN* of Ag–Ag and Ag–Au were 3.6 and 3.4 with the bond length at 2.85 and 2.81 Å, respectively. However, there was still part of Ag remaining at oxidative state, which was proved by the data fitting of EXAFS data, as shown in Table 1, the *CN* of Ag–O was 1.5. This might be contributed by the strong interaction between Ag and the silica support and the oxidation of Ag by air. When the catalyst reduced in situ under H_2 atmosphere, more Au–Ag interaction occurred: the *CN* of Au–Ag and Ag–Au increased from 1.2 to 3.6 and from 3.4 to 6.3, respectively (Table 1). Only very few Ag–O (CN: ~0.5) interaction remained, which may act as nano-glue that anchor Au–Ag alloy nanoparticles onto the surface of silica support [25,35].

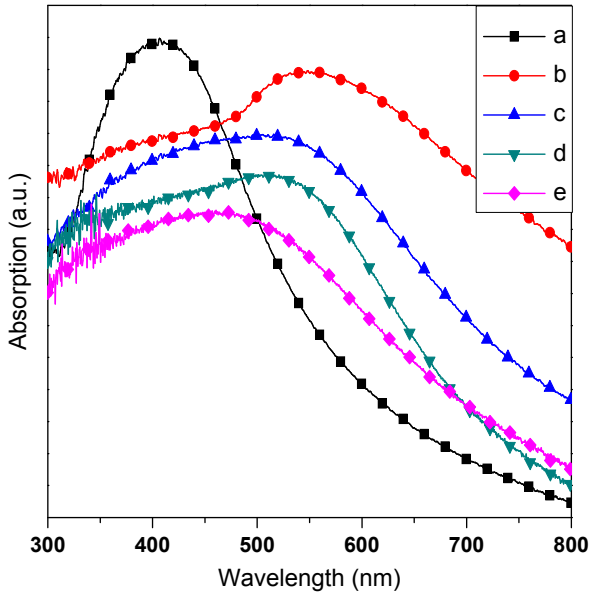

Fig. 4 The UV–vis spectra of the Au–Ag/SiO_2: (a–e) are corresponding to those in Fig. 1. The position of the surface plasma resonance peaks: (a) 406 nm; (b) 550 nm; (c) 440 and 525 nm; (d) 520 nm; and (e) 468 nm.

3.5. *Catalytic performance of the Au–Ag/SiO_2 catalyst*

PROX is an important reaction for purification of H_2 for fuel cells applications. Thus, we applied the above Au–Ag/SiO_2 catalyst to this reaction. The catalytic performance of PROX is shown in Fig. 6. With increasing temperature, the conversion and selectivity of the catalyst are all decreased due to the competitive oxidation of H_2. Surprisingly, the catalytic performance in PROX reaction over the catalyst in this work is very close to that of the Au–Ag/SiO_2 catalyst in our previous work [25], where the particle size of Au–Ag alloy nanoparticles were much smaller than that in this work. They were all superior to the corresponding monometallic ones. This result manifested that the particle size effect of Au–Ag nanoparticles is not as important as that of monometallic gold. The formation of Au–Ag alloy stabilized the nanoparticle and made it less sensitive to the particle size.

4. Discussions

4.1. *Formation mechanism of Au–Ag/SiO_2 catalyst*

From the above results, we propose that the formation process of Au–Ag alloy nanoparticles supported on silica by galvanic

Table 1 Analysis results of the EXAFS data at Au L_{III}-edge and Ag K-edge. (a–e) are corresponding to those in Fig. 1.

Edge	Sample	Shell	*CN*	*R* (Å)	$\sigma^2 \times 10^2$ (Å^2)	ΔE_0 (eV)	*r*-Factor (%)
Au L_{III}-edge	Au foil	Au–Au	12	2.86	0.77	3.1	0.38
	b	Au–Au	11.6	2.85	0.77	2.6	0.38
	c	Au–Au	10.8	2.83	1.07	1.6	0.38
		Au–Ag	1.1	2.81	1.07	1.6	
	d	Au–Au	10.4	2.84	0.98	1.6	0.33
		Au–Ag	1.2	2.81	0.98	1.6	
	e	Au–Au	8.3	2.83	0.99	1.6	0.22
		Au–Ag	3.6	2.83	1.04	1.6	
Ag K-edge	Ag foil	Ag–Ag	12	2.86	0.91	9.2	0.12
	a	Ag–O	1.0	2.13	0.38	1.4	0.37
		Ag–Ag	4.4	2.85	1.04	−0.62	
	b	Ag–Cl	5.3	2.70	1.77	−1.75	0.50
		Ag–Ag	1.3	3.06	1.77	−1.75	
	c	Ag–O	1.1	2.23	1.29	0.16	0.37
		Ag–Ag	4.9	2.85	1.13	0.16	
		Ag–Au	2.3	2.81	0.81	0.16	
	d	Ag–O	1.5	2.26	1.26	−1.76	0.33
		Ag–Ag	3.6	2.85	1.18	−1.76	
		Ag–Au	3.4	2.81	1.18	−1.76	
	e	Ag–O	0.5	2.24	1.68	−0.66	0.22
		Ag–Ag	3.9	2.84	0.94	−0.66	
		Ag–Au	6.3	2.83	0.92	−0.66	

CN, the coordination number for the absorber–backscatterer pair. *R*, the average absorber–backscatterer distance. σ^2, the Debye–Waller factor. ΔE_0, the inner potential correction.

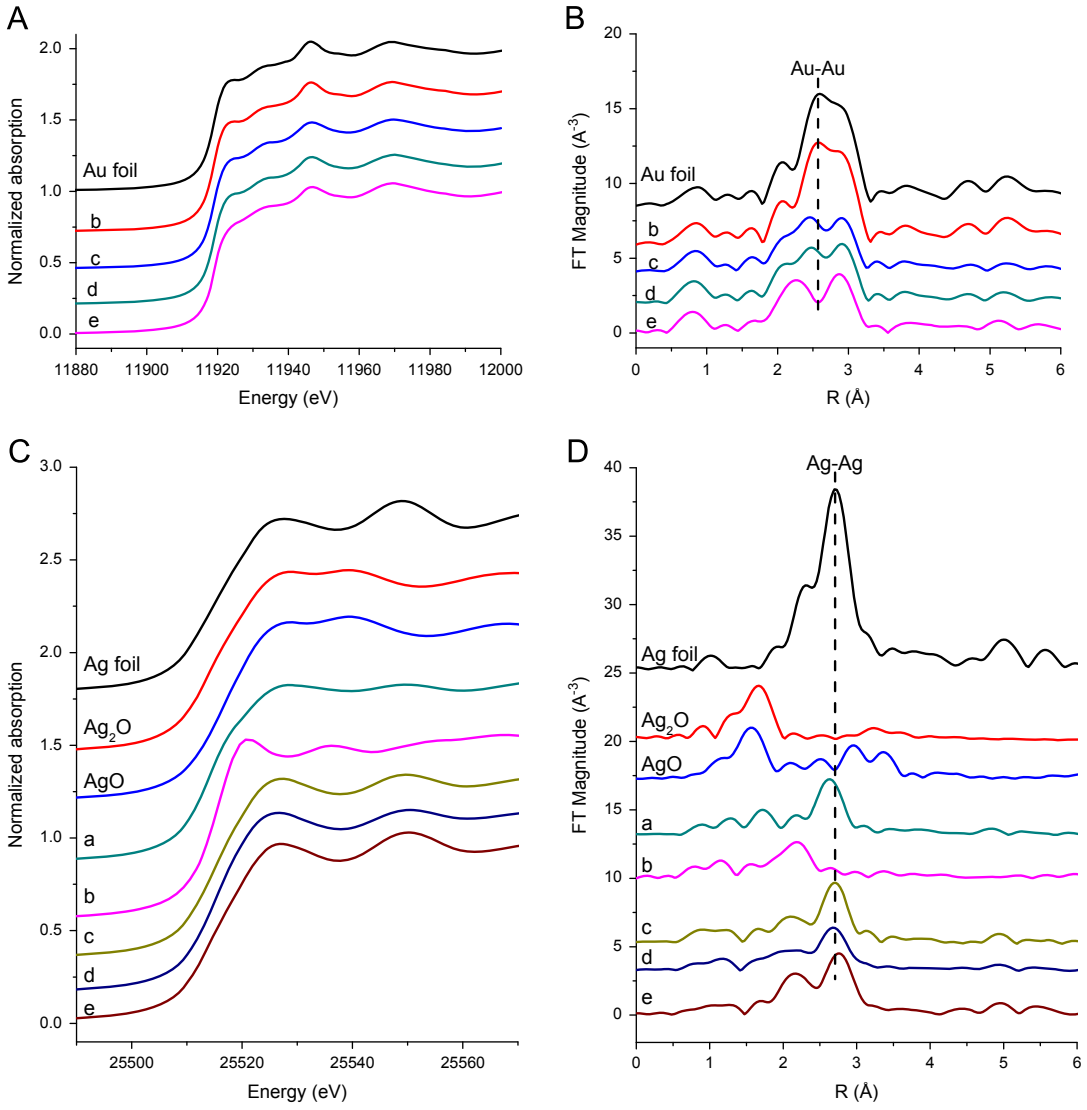

Fig. 5 Normalized XANES spectra (A, C) and Fourier transform of k^3-weighted EXAFS spectra (without phase correction) (B, D) at the Au L_{III}-edge (A, B) and Ag K-edge (C, D) of the Au–Ag/SiO_2 catalyst. (a–e) are corresponding to those in Fig. 1.

replacement reaction can be described by the following equations:

$$2(-NH_2)+Ag^+=[(-NH_2)_2Ag]^+ \quad (1)$$

$$2[(-NH_2)_2Ag]^++2BH_4^-+6H_2O=2Ag+2H_3BO_3+7H_2+4(-NH_2) \quad (2)$$

$$3Ag+AuCl_4^-=3AgCl+Au+Cl^- \quad (3)$$

$$(-NH_2)+H^++AuCl_4^-=(-NH_3)^+AuCl_4^- \quad (4)$$

$$2(-NH_3)^+AuCl_4^-+8BH_4^-+24H_2O=2Au+8Cl^-+8H_3BO_3+29H_2+2(-NH_2) \quad (5)$$

$$2AgCl+2BH_4^-+6H_2O=2Ag+2Cl^-+2H_3BO_3+7H_2 \quad (6)$$

Sample (a) was obtained by reactions (1)–(2). The residual $NaBH_4$ reacted with water and produced H_3BO_3 and H_2. After filtration and washing, the residual Na^+ or H_3BO_3 would be washed off. At this step, highly dispersed Ag nanoparticles were formed on the surface of silica gel, as shown in Fig. 1a. In the second step, $HAuCl_4$ was added. Metallic Au and Ag was produced via reaction (3), and the excess $HAuCl_4$ was attached to the surface of silica via reaction (4). According to the XRD and TEM results, at this step, relatively big gold nanoparticles and AgCl were formed, as depicted in Fig. 1b. The formation of AgCl produced by reaction (3) might lead to the growth of the Au–Ag alloy nanoparticles, which made the average size of the Au–Ag alloy nanoparticles in this work larger than loading Au first as in our previous work [25]. After $NaBH_4$ was added, the residual $AuCl_4^-$ and AgCl was reduced to metallic state and part of them even formed Au–Ag alloy via reactions (5) and (6), respectively. According to the UV–vis and XAS results, there is some Au–Ag alloy formed besides the monometallic Au and Ag, as shown in Fig. 1c. The organic ligands (APTES) was removed by the calcination process, which led to strong interaction between Ag and SiO_2 at the same time. There was Au–Ag alloy phase with less Ag compared with that after high temperature reduction, according to the UV–vis and EXAFS data fitting results. Since Ag interacts with oxygen much more strongly than that with Au, the AgO_x would enrich on the shell of the particles, as shown in Fig. 1d. After high temperature reduction, Au–Ag alloy nanoparticles was formed (Fig. 1e). The average particle size of Au–Ag alloy in this

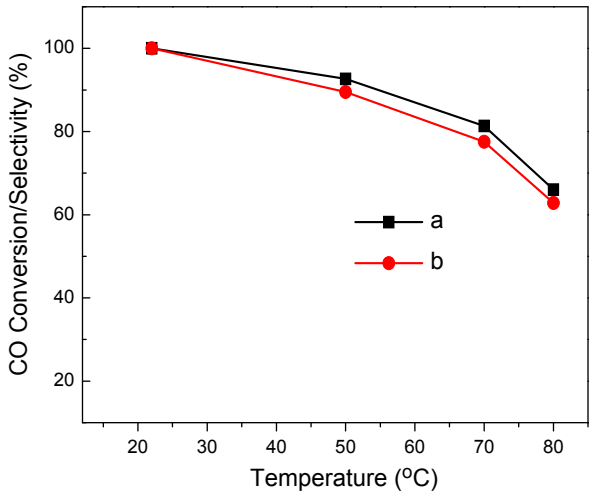

Fig. 6 CO conversion/selectivity in PROX reaction with temperature over the Au–Ag alloy catalyst obtained with different loading procedures. The Au–Ag/SiO_2 catalyst in this work (a) and our previous work (b) in Ref. [25]. In each experiment, 60 mg of the catalyst was used. Gas mixture: $CO/O_2/H_2/He = 1/1/60/38$ (vol.); flow rate: 40 mL min^{-1}.

work was much smaller than those synthesized by the one pot method [17], which indicate that the two step method in a reversed way was much more efficient in controlling the size of Au–Ag alloy nanoparticles than the one pot method. In galvanic replacement reaction, for every Au(0), three Ag atoms are replaced which means that the size of the nanoparticle would be decreased. On the other hand, normal Ostwald rippening would help increasing the particle sizes [31]. Because of the presence of an excess $-NH_2$ on the surfaces of silica, the dissolution-regrowth process in Ostwald rippening was effectively suppressed. As a result, we have a situation of two-size distribution of the alloy nanoparticles.

4.2. *Origin of the catalytic activity of Au–Ag/SiO_2 catalyst*

Generally, the activities of supported gold nanocatalysts are very sensitive to the particle size. Much effort has been made in the control of the size of gold nanoparticles [36–38]. However, this is not the case in all the gold-based bimetallic systems. For example, Iizuka et al. found that Au powders (~166 nm) with some Ag impurities exhibited better catalytic activity than pure Au powders [39]. Zhou et al. [40] decorated gold film whose crystal grains were tens and hundreds of nanometers with CeO_2 nanoparticles (less than 5 nm) and found that the catalytic activity in CO oxidation was enhanced a lot. They showed that gold atoms/ions at the interface with ceria nanoparticles were the active sites. So the optimal size of gold nanoparticles is not the main reason that leads to the high catalytic activity. The foam like nanoporous gold (NPG) catalyst generated by silver leaching of Au–Ag alloys also showed excellent catalytic activity in CO oxidation [41,42]. The minuet residual silver on the gold plays a vital role in enhancing the catalytic performances [43–45]. The intimate interaction between gold and silver is more important than the particle size of gold itself. The synergy effect mainly stems from the adsorption and activation of CO and O_2 on neighboring gold and silver atoms, respectively. Recently, Fujita et al. [45] observed Ag-stabilized Au atomic steps and kinks on the curved surfaces of NPG, comparable to 3–5 nm nanoparticles which are responsible for the high catalytic oxidation of CO. In our catalyst, although the particle sizes of the Au–Ag alloy nanoparticles are not as small and uniform as the previous ones [25], the catalytic activity remained very high. Thus, the Au–Ag/SiO_2 catalyst give high catalytic activity while it is less sensitive to the particle size than the monometallic Au/SiO_2.

5. Conclusions

Au–Ag alloy nanoparticles supported on silica was synthesized via galvanic replacement reaction. The results of XRD, TEM, UV–vis and XAS demonstrated that AgCl was formed during the reaction, which might be the main reason that led to the growth of Au–Ag alloy nanoparticles. Although with larger particle size, the Au–Ag/SiO_2 catalyst in this work exhibited excellent catalytic activity in PROX reaction similar to that with small particle size in our previous work [25]. The origin of the intrinsic activity is from the intimate interaction between Au and Ag after formation of Au–Ag alloy nanoparticles. This result provides further evidence for the insensitivity of catalytic activity of the Au–Ag alloy to the particle size, which also can be extended to other gold-based systems.

Acknowledgments

This work was supported by grants from National Natural Science Foundation of China (NSFC No. 21176235), "Hundred Talents Program of Dalian Institute of Chemical Physics (DICP)" and from the National Science Council, Taiwan (NSC 98-2120-M-002-002) and National Taiwan University for a postdoctoral fellowship (X. Liu).

References

[1] A. Murugadoss, N. Kai, H. Sakurai, Synthesis of bimetallic gold-silver alloy nanoclusters by simple mortar grinding, Nanoscale 4 (2012) 1280–1282.
[2] P. Pinkhasova, L. Yang, Y. Zhang, S. Sukhishvili, H. Du, Differential SERS activity of gold and silver nanostructures enabled by adsorbed poly(vinylpyrrolidone), Langmuir 28 (2012) 2529–2535.
[3] S.Y. Li, M. Wang, A novel SERS-active tag based on bimetallic flowerlike Au–Ag nanoparticles, Current Nanoscience 7 (2011) 969–978.
[4] A.Y. Sonay, A.B. Caglayan, M. Culha, Synthesis of peptide mediated Au core–Ag shell nanoparticles as surface-enhanced Raman scattering labels, Plasmonics 7 (2012) 77–86.
[5] D.Y. Zheng, C.G. Hu, T.A. Gan, X.P. Dang, S.S. Hu, Preparation and application of a novel vanillin sensor based on biosynthesis of Au–Ag alloy nanoparticles, Sensors & Actuators, B: Chemical 148 (2010) 247–252.
[6] H. He, X. Xu, H. Wu, Y. Jin, Enzymatic plasmonic engineering of Ag/Au bimetallic nanoshells and their use for sensitive optical glucose sensing, Advanced Materials 24 (2012) 1736–1740.
[7] N.K. Chaki, H. Tsunoyama, Y. Negishi, H. Sakurai, T. Tsukuda, Effect of Ag-doping on the catalytic activity of polymer-stabilized Au clusters in aerobic oxidation of alcohol, Journal of Physical Chemistry C 111 (2007) 4885–4888.
[8] D. Tsukamoto, A. Shiro, Y. Shiraishi, Y. Sugano, S. Ichikawa, S. Tanaka, T. Hirai, Photocatalytic H_2O_2 production from ethanol/O_2 system using TiO_2 loaded with Au–Ag bimetallic alloy nanoparticles, ACS Catalysis 2 (2012) 599–603.
[9] J. Park, J. Joo, S.G. Kwon, Y. Jang, T. Hyeon, Synthesis of monodisperse spherical nanocrystals, Angewandte Chemie International Edition 46 (2007) 4630–4660.
[10] Y.-H. Chen, C.-S. Yeh, A new approach for the formation of alloy nanoparticles: laser synthesis of gold–silver alloy from gold–silver colloidal mixtures, Chemical Communications (2001) 371–372.

[11] J.P. Wilcoxon, P.P. Provencio, Heterogeneous growth of metal clusters from solutions of seed nanoparticles, Journal of the American Chemical Society 126 (2004) 6402–6408.
[12] D. Wang, Y. Li, Bimetallic nanocrystals: liquid-phase synthesis and catalytic applications, Advanced Materials 23 (2011) 1044–1060.
[13] M.P. Mallin, C.J. Murphy, Solution-phase synthesis of sub-10 nm Au–Ag alloy nanoparticles, Nano Letters 2 (2002) 1235–1237.
[14] J.P. Wilcoxon, B.L. Abrams, Synthesis, structure and properties of metal nanoclusters, Chemical Society Reviews 35 (2006) 1162.
[15] L. Au, X. Lu, Y. Xia, A comparative study of galvanic replacement reactions involving Ag nanocubes and $AuCl_2^-$ or $AuCl_4^-$, Advanced Materials 20 (2008) 2517–2522.
[16] M. Haruta, T. Kobayashi, H. Sano, N. Yamada, Novel gold catalysts for the oxidation of carbon-monoxide at a temperature far below 0 °C, Chemistry Letters (1987) 405–408.
[17] J.H. Liu, A.Q. Wang, Y.S. Chi, H.P. Lin, C.Y. Mou, Synergistic effect in an Au–Ag alloy nanocatalyst: CO oxidation, Journal of Physical Chemistry B 109 (2005) 40–43.
[18] W. Li, A. Wang, X. Liu, T. Zhang, Silica-supported Au–Cu alloy nanoparticles as an efficient catalyst for selective oxidation of alcohols, Applied Catalysis A: General 433–434 (2012) 146–151.
[19] X. Liu, Y. Li, J.W. Lee, C.Y. Hong, C.Y. Mou, B.W.L. Jang, Selective hydrogenation of acetylene in excess ethylene over SiO_2 supported Au–Ag bimetallic catalyst, Applied Catalysis A: General 439 (2012) 8–14.
[20] A. Veres, T. Rica, L. Janovak, M. Doemoek, N. Buzas, V. Zollmer, T. Seemann, A. Richardt, I. Dekany, Silver and gold modified plasmonic TiO_2 hybrid films for photocatalytic decomposition of ethanol under visible light, Catalysis Today 181 (2012) 156–162.
[21] A.Q. Wang, J.H. Liu, S.D. Lin, T.S. Lin, C.Y. Mou, A novel efficient Au–Ag alloy catalyst system: preparation, activity, and characterization, Journal of Catalysis 233 (2005) 186–197.
[22] A.Q. Wang, C.M. Chang, C.Y. Mou, Evolution of catalytic activity of Au–Ag bimetallic nanoparticles on mesoporous support for CO oxidation, Journal of Physical Chemistry B 109 (2005) 18860–18867.
[23] A.Q. Wang, Y. Hsieh, Y.F. Chen, C.Y. Mou, Au–Ag alloy nanoparticle as catalyst for CO oxidation: effect of Si/Al ratio of mesoporous support, Journal of Catalysis 237 (2006) 197–206.
[24] C.W. Yen, M.L. Lin, A.Q. Wang, S.A. Chen, J.M. Chen, C.Y. Mou, CO oxidation catalyzed by Au–Ag bimetallic nanoparticles supported in mesoporous silica, Journal of Physical Chemistry C 113 (2009) 17831–17839.
[25] X.Y. Liu, A.Q. Wang, X.F. Yang, T. Zhang, C.Y. Mou, D.S. Su, J. Li, Synthesis of thermally stable and highly active bimetallic Au–Ag nanoparticles on inert supports, Chemistry of Materials 21 (2009) 410–418.
[26] A. Sandoval, A. Aguilar, C. Louis, A. Traverse, R. Zanella, Bimetallic Au–Ag/TiO_2 catalyst prepared by deposition-precipitation: high activity and stability in CO oxidation, Journal of Catalysis 281 (2011) 40–49.
[27] Y. Sun, Y.N. Xia, Shape-controlled synthesis of gold and silver nanoparticles, Science 298 (2002) 2176–2179.
[28] V. Bansal, H. Jani, J. Du Plessis, P.J. Coloe, S.K. Bhargava, Galvanic replacement reaction on metal films: a one-step approach to create nanoporous surfaces for catalysis, Advanced Materials 20 (2008) 717–723.
[29] H.P. Liang, Y.G. Guo, H.M. Zhang, J.S. Hu, L.J. Wan, C.L. Bai, Controllable AuPt bimetallic hollow nanostructures, Chemical Communications (2004) 1496–1497.
[30] B. Ravel, M. Newville, ATHENA, ARTEMIS, HEPHAESTUS: data analysis for X-ray absorption spectroscopy using IFEFFIT, Journal of Synchrotron Radiation 12 (2005) 537–541.
[31] X. Lu, H.Y. Tuan, J. Chen, Z.Y. Li, B.A. Korgel, Y. Xia, Mechanistic studies on the galvanic replacement reaction between multiply twinned particles of Ag and $HAuCl_4$ in an organic medium, Journal of the American Chemical Society 129 (2007) 1733–1742.
[32] P.-H. Liu, Y.-P. Chang, T.-H. Phan, K.-J. Chao, The morphology and size of nanostructured Au in Au/SBA-15 affected by preparation conditions, Materials Science and Engineering: C 26 (2006) 1017–1022.
[33] A.I. Frenkel, C.W. Hills, R.G. Nuzzo, A view from the inside: complexity in the atomic scale ordering of supported metal nanoparticles, Journal of Physical Chemistry B 105 (2001) 12689–12703.
[34] J.T. Miller, A.J. Kropf, Y. Zha, J.R. Regalbuto, L. Delannoy, C. Louis, E. Bus, J.A. van Bokhoven, The effect of gold particle size on Au–Au bond length and reactivity toward oxygen in supported catalysts, Journal of Catalysis 240 (2006) 222–234.
[35] X.Y. Liu, A.Q. Wang, L. Li, T. Zhang, C.Y. Mou, J.F. Lee, Structural changes of Au–Cu bimetallic catalysts in CO oxidation: in situ XRD, EPR, XANES, and FT-IR characterizations, Journal of Catalysis 278 (2011) 288–296.
[36] Y. Liu, C.J. Jia, J. Yamasaki, O. Terasaki, F. Schuth, Highly active iron oxide supported gold catalysts for CO oxidation: how small must the gold nanoparticles be?, Angewandte Chemie International Edition 49 (2010) 5771–5775.
[37] M.S. Chen, D.W. Goodman, The structure of catalytically active gold on titania, Science 306 (2004) 252–255.
[38] M. Haruta, Size- and support-dependency in the catalysis of gold, Catalysis Today 36 (1997) 153–166.
[39] Y. Iizuka, T. Miyamae, T. Miura, M. Okumura, M. Daté, M. Haruta, A kinetic study on the low temperature oxidation of CO over Ag-contaminated Au fine powder, Journal of Catalysis 262 (2009) 280–286.
[40] Z. Zhou, M. Flytzani-Stephanopoulos, H. Saltsburg, Decoration with ceria nanoparticles activates inert gold island/film surfaces for the CO oxidation reaction, Journal of Catalysis 280 (2011) 255–263.
[41] B. Jurgens, C. Kubel, C. Schulz, T. Nowitzki, V. Zielasek, J. Biener, M.M. Biener, A.V. Hamza, M. Baumer, New gold and silver–gold catalysts in the shape of sponges and sieves, Gold Bulletin 40 (2007) 142–149.
[42] V. Zielasek, B. Jurgens, C. Schulz, J. Biener, M.M. Biener, A.V. Hamza, M. Baumer, Gold catalysts: nanoporous gold foams, Angewandte Chemie International Edition 45 (2006) 8241–8244.
[43] M. Haruta, New generation of gold catalysts: nanoporous foams and tubes—is unsupported gold catalytically active?, ChemPhysChem 8 (2007) 1911–1913.
[44] A. Wittstock, B. Neumann, A. Schaefer, K. Dumbuya, C. Kubel, M.M. Biener, V. Zielasek, H.P. Steinruck, J.M. Gottfried, J. Biener, A. Hamza, M. Baumer, Nanoporous Au: an unsupported pure gold satalyst?, Journal of Physical Chemistry C 113 (2009) 5593–5600.
[45] T. Fujita, P. Guan, K. McKenna, X. Lang, A. Hirata, L. Zhang, T. Tokunaga, S. Arai, Y. Yamamoto, N. Tanaka, Y. Ishikawa, N. Asao, Y. Yamamoto, J. Erlebacher, M. Chen, Atomic origins of the high catalytic activity of nanoporous gold, Nature Materials 11 (2012) 775–780.